Transversity from Single-Hadron TSSAs and Dihadron Fragmentation Theory Developments

Daniel Pitonyak[a]

[a]*Department of Physics, Lebanon Valley College,*
Annville, Pennsylvania, USA

E-mail: pitonyak@lvc.edu

I report on a QCD global analysis of transverse single-spin asymmetries (TSSAs) involving transverse momentum dependent (TMD)/collinear twist-3 (CT3) observables where single-hadron fragmentation functions (FFs) enter. I further explore the impact of lattice QCD tensor charge calculations on the results. A byproduct of this study is the extraction of the transversity PDFs and calculation of the nucleon tensor charges, where comparisons are made to previous phenomenological analyses. I also discuss new developments in the theory of dihadron fragmentation functions (DiFFs), where a definition is introduced that maintains a number density interpretation in a parton model framework (just as one has for single-hadron FFs). The associated evolution equations for these DiFFs are also derived.

1. Background on TSSAs

Mapping the 3-dimensional structure of hadrons relies crucially on understanding phenomena sensitive to the transverse spin of hadrons and/or partons. These observables probe novel intrinsic parton motion and quark-gluon-quark correlations in hadrons. From a theoretical standpoint, two main frameworks have been developed to describe these data sets. For processes with two scales $\Lambda_{QCD} \sim q_T \ll Q$, one uses transverse momentum dependent (TMD) factorization. If an observable is only sensitive to one large scale $Q \gg \Lambda_{QCD}$, then one can employ collinear factorization, whose non-perturbative objects depend only on the lightcone momentum fractions carried by the partons. In the case of TSSAs, the collinear PDFs and FFs are subleading twist (twist-3) and encode quark-gluon-quark correlations in hadrons. These two frameworks do not exist in isolation from each other and have been shown in previous theoretical calculations to agree in their overlapping region of validity $\Lambda_{QCD} \ll q_T \ll Q$.

The `JAM3D-22` global analysis [1] included the Sivers $A_{UT}^{\sin(\phi_h - \phi_S)}$, Collins $A_{UT}^{\sin(\phi_h + \phi_S)}$, and $A_{UT}^{\sin \phi_S}$ asymmetries in SIDIS, Collins asymmetry in SIA for so-called unlike-like (A_{UL}) and unlike-charged (A_{UC}) ratios, Sivers asymmetry in DY for $W^\pm/Z$ production ($A_N^{W/Z}$) and for $\mu^+\mu^-$ production ($A_{T,\mu^+\mu^-}^{\sin \phi_S}$), and A_N for pion production in proton-proton collisions (A_N^π). More details on the parton model framework for these observables can be found in Ref. [1]. In addition, we also imposed the Soffer bound on transversity and used information from lattice QCD on the nucleon tensor charges as priors in our fit. These charges are not only relevant for QCD phenomenology and lattice QCD but also model calculations as well as low-energy beyond the Standard Model physics – see Refs. [2–10] for details.

2. JAM3D-22 Global Analysis of TSSAs

2.1 Methodology

We employ a Gaussian ansatz in transverse momentum space and decouple the x and k_T (z and p_T) dependence. For the unpolarized and transversity TMDs we have

$$f^q(x, \vec{k}_T^2) = f^q(x)\, \mathcal{G}_f^q(k_T^2), \tag{1}$$

where the generic function $f = f_1$ or h_1, and

$$\mathcal{G}_f^q(k_T^2) = \frac{1}{\pi \langle k_T^2 \rangle_f^q} \exp\left[-\frac{k_T^2}{\langle k_T^2 \rangle_f^q}\right], \tag{2}$$

with $k_T \equiv |\vec{k}_T|$. Using the relation $\pi F_{FT}(x, x) = f_{1T}^{\perp(1)}(x)$, the Sivers function reads

$$f_{1T}^{\perp q}(x, \vec{k}_T^2) = \frac{2M^2}{\langle k_T^2 \rangle_{f_{1T}^\perp}^q} \pi F_{FT}(x, x)\, \mathcal{G}_{f_{1T}^\perp}^q(k_T^2). \tag{3}$$

For the TMD FFs, the unpolarized function is parametrized as

$$D_1^{h/q}(z, z^2 \vec{p}_T^2) = D_1^{h/q}(z)\, \mathcal{G}_{D_1}^{h/q}(z^2 p_T^2), \tag{4}$$

while the Collins FF reads

$$H_1^{\perp h/q}(z, z^2 \vec{p}_T^2) = \frac{2z^2 M_h^2}{\langle P_\perp^2 \rangle_{H_1^\perp}^{h/q}} H_{1\,h/q}^{\perp(1)}(z)\, \mathcal{G}_{H_1^\perp}^{h/q}(z^2 p_T^2), \tag{5}$$

where we have explicitly written its z dependence in terms of its first moment $H_{1\,h/q}^{\perp(1)}(z)$. The widths for the FFs are denoted as $\langle P_\perp^2 \rangle_D^{h/q}$, where $D = D_1$ or $H_1^\perp$. (Note that the hadron transverse momentum $\vec{P}_\perp$ with respect to the fragmenting quark is $\vec{P}_\perp = -z\vec{p}_T$.) For $f_1^q(x)$ and $D_1^{h/q}(z)$ we use the leading-order CJ15 [11] and DSS [12] functions. The pion PDFs are taken from Ref. [13] and are next-to-leading order.

We generically parametrize the collinear functions $h_1(x)$, $F_{FT}(x, x)$, $H_1^{\perp(1)}(z)$, $\tilde{H}(z)$, at an initial scale of $Q_0^2 = 2\,\text{GeV}^2$, as

$$F^q(x) = \frac{N_q\, x^{a_q}(1-x)^{b_q}(1 + \gamma_q\, x^{\alpha_q}(1-x)^{\beta_q})}{\text{B}[a_q+2, b_q+1] + \gamma_q \text{B}[a_q+\alpha_q+2, b_q+\beta_q+1]}, \tag{6}$$

where $F^q = h_1^q, \pi F_{FT}^q, H_{1\,h/q}^{\perp(1)}, \tilde{H}^{h/q}$ (with $x \to z$ for the latter two functions), and B is the Euler beta function. We also implement a DGLAP-type evolution for the collinear part of these functions, analogous to Ref. [14], where a double-logarithmic Q^2-dependent term is explicitly added to the parameters. For the collinear PDFs $h_1^q(x)$ and $\pi F_{FT}^q(x, x)$, we only allow $q = u, d$ and set antiquark functions to zero. Nevertheless, the u and d functions are understood as being the sum of valence and sea contributions, i.e., $u = u_v + \bar{u}$ and $d = d_v + \bar{d}$. For both functions, $\{\gamma, \alpha, \beta\}$ are not used, and we set $b_u = b_d$, as the χ^2/npts does not improve by leaving more parameters free. For the collinear FFs $H_{1\,h/q}^{\perp(1)}(z)$ and $\tilde{H}^{h/q}(z)$, we allow for favored (fav) and unfavored (unf) parameters, with fav corresponding to the fragmentation channels $u \to \pi^+$, $\bar{d} \to \pi^+$ ($\bar{u} \to \pi^-$, $d \to \pi^-$) and unf for all other flavors. For $H_{1\,h/q}^{\perp(1)}(z)$, $\{\gamma, \beta\}$ are free while α is set to zero. This is due to the change in shape of the SIA data as a function of z and the fact that the data are at larger $z > 0.2$. For $\tilde{H}^{h/q}(z)$, $\{\gamma, \alpha, \beta\}$ are not used, and we set $a_{fav} = a_{unf}$ and $b_{fav} = b_{unf}$. We have verified that no meaningful change in the χ^2/npts occurs if a and b are separately fit for favored and unfavored, as the SIDIS and A_N data are not sensitive enough to $\tilde{H}^{h/q}(z)$ to constrain more free parameters.

In the end we have a total of 24 parameters for the collinear functions. There are also 4 parameters for the transverse momentum widths associated with h_1, $f_{1T}^\perp$, and $H_1^\perp$: $\langle k_T^2 \rangle_{f_{1T}^\perp}^u = \langle k_T^2 \rangle_{f_{1T}^\perp}^d \equiv \langle k_T^2 \rangle_{f_{1T}^\perp}$; $\langle k_T^2 \rangle_{h_1}^u = \langle k_T^2 \rangle_{h_1}^d \equiv \langle k_T^2 \rangle_{h_1}$; $\langle P_\perp^2 \rangle_{H_1^\perp}^{fav}$ and $\langle P_\perp^2 \rangle_{H_1^\perp}^{unf}$. We extract the unpolarized TMD widths by including HERMES pion and kaon multiplicities, which involves 6 more parameters: $\langle k_T^2 \rangle_{f_1}^{val}$, $\langle k_T^2 \rangle_{f_1}^{sea}$, $\langle P_\perp^2 \rangle_{D_1^\pi}^{fav}$, $\langle P_\perp^2 \rangle_{D_1^\pi}^{unf}$, $\langle P_\perp^2 \rangle_{D_1^K}^{fav}$, $\langle P_\perp^2 \rangle_{D_1^K}^{unf}$. Our working hypothesis for the pion PDF widths is that they are the same as those for the proton. The JAM Monte Carlo framework is used to sample the Bayesian posterior distribution with approximately 500 replicas of the parameters in order to estimate uncertainties for our extracted non-perturbative quantities.

We enforce the Soffer bound (SB) $2|h_1(x)| \le (f_1(x) + g_1(x))$ by generating "data" at a scale of $Q_0^2 = 2\,\text{GeV}^2$ for the r.h.s. for $0 < x < 1$ using the unpolarized and helicity PDFs from Ref. [15]. The fact that $f_1(x)$ and $g_1(x)$ were extracted in Ref. [15] simultaneously using Monte Carlo methods allows us to use their replicas to calculate a central value and 1-σ uncertainty for the r.h.s. at a given x. This SB data is then included in our analysis as an additional constraint. However, the theory

Observable	Reactions	χ^2/npts
$A_{UT}^{\sin(\phi_h-\phi_S)}$	$e + (p,d)^\uparrow \rightarrow e + (\pi^+, \pi^-, \pi^0) + X$	$182.9/166 = 1.10$
$A_{UT}^{\sin(\phi_h+\phi_S)}$	$e + (p,d)^\uparrow \rightarrow e + (\pi^+, \pi^-, \pi^0) + X$	$181.0/166 = 1.09$
$^*A_{UT}^{\sin\phi_S}$	$e + p^\uparrow \rightarrow e + (\pi^+, \pi^-, \pi^0) + X$	$18.6/36 = 0.52$
$A_{UC/UL}$	$e^+ + e^- \rightarrow \pi^+\pi^- (UC, UL) + X$	$154.9/176 = 0.88$
$A_{T,\mu^+\mu^-}^{\sin\phi_S}$	$\pi^- + p^\uparrow \rightarrow \mu^+\mu^- + X$	$6.92/12 = 0.58$
$A_N^{W/Z}$	$p^\uparrow + p \rightarrow (W^+, W^-, Z) + X$	$30.8/17 = 1.81$
A_N^π	$p^\uparrow + p \rightarrow (\pi^+, \pi^-, \pi^0) + X$	$70.4/60 = 1.17$
Lattice g_T	——	$1.82/1 = 1.82$

Table 1: Summary of the observables analyzed in `JAM3D-22` . There are a total of 21 different reactions. There are also a total of 8 non-perturbative functions when one takes into account flavor separation. The χ^2 is computed based on calculating for each point the theory expectation value from the replicas. *For the $A_{UT}^{\sin\phi_S}$ data we only use the x- and z-projections.

calculation of $|h_1(x)|$, point-by-point in x, only contributes to the overall χ^2 if the l.h.s. violates the inequality with the generated SB data on the r.h.s. by more than 1-σ.

2.2 Extracted Non-Perturbative Functions

Our simultaneous global analysis of TSSAs (`JAM3D-22`) includes all the observables in Table 1. The overall χ^2/npts is 1.02. The cuts of $0.2 < z < 0.6$, $Q^2 > 1.63\,\text{GeV}^2$, and $0.2 < P_{hT} < 0.9\,\text{GeV}$ have been applied to all SIDIS data sets and $P_{hT} > 1\,\text{GeV}$ to all A_N^π data sets.

The non-perturbative functions extracted from our analysis can be found in a `Google Colab` notebook [16] as well as LHAPDF tables [17]. The comparison of our `JAM3D-22` non-perturbative functions with those from other groups is shown in Fig. 1. Now that the Soffer bound is imposed in `JAM3D-22`, $h_1^d(x)$ matches more closely to other extractions. However, a striking difference is still the large size of $h_1^u(x)$ in `JAM3D-22` that now saturates the Soffer bound at $x \gtrsim 0.35$. This is necessary to not only describe the lattice g_T data point but also the A_N^π measurements. Without including this information in the analysis (i.e., relying only on the standard TMD or dihadron observables that are typically used to extract transversity), one does not find this solution for $h_1^u(x)$. This function can actually describe all relevant TSSAs considered here (TMD *and* collinear twist-3) sensitive to transversity as well as obtain agreement with lattice tensor charge values.

2.3 Tensor Charges

From the transversity function we are able to calculate the tensor charges δu, δd, and g_T using

$$\delta u = \int_0^1 dx \left(h_1^u(x) - h_1^{\bar u}(x) \right), \qquad \delta d = \int_0^1 dx \left(h_1^d(x) - h_1^{\bar d}(x) \right), \qquad g_T \equiv \delta_u - \delta_d. \qquad (7)$$

For `JAM3D-22` we find $\delta u = 0.78 \pm 0.11$, $\delta d = -0.12 \pm 0.11$, and $g_T = 0.90 \pm 0.05$. These results are shown in Fig. 2 compared to an analysis that does not include the lattice g_T data point (`JAM3D-22` no LQCD) and the `JAM3D-20+` fit as well as the computations from other phenomenological, lattice QCD, and Dyson-Schwinger studies. The inclusion of the precise lattice QCD data point for g_T
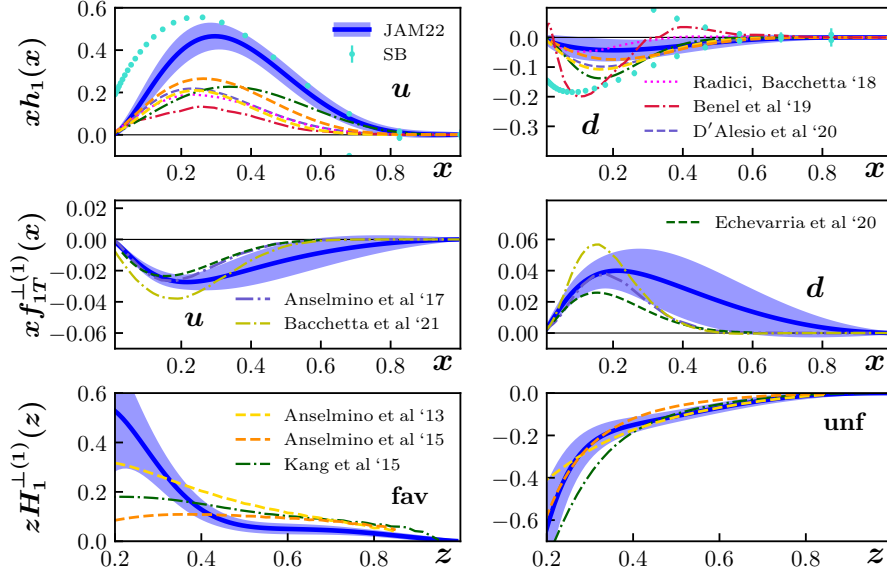
Figure 1: The extracted functions $h_1(x)$, $f_{1T}^{\perp(1)}(x)$, and $H_1^{\perp(1)}(z)$ at $Q^2 = 4$ GeV^2 from our `JAM3D-22` global analysis (blue solid curves with 1-σ CL error bands) compared to the functions from other groups. The generated Soffer bound (SB) data are also displayed (cyan points). We note that for all groups the curves are the central values of the 68% confidence band. The transversity function for Radici, Bacchetta '18 and Benel, Courtoy, Ferro-Hernandez '20 are for valence u and d quarks.

from Ref. [18] (Alexandrou, et al. (2020) in Fig. 2) causes a substantial reduction in the uncertainty for $\delta u, \delta d$, and g_T. Previous extractions [19–24] typically fell below the lattice results for δu and g_T, even when relaxing the Soffer bound constraint [23, 24].

The imposition of the Soffer bound in our `JAM3D-22` global analysis restricts the size of transversity, especially for the down quark. In addition, now that the $\tilde{H}(z)$ term in A_N^π is not set to zero, $h_1^u(x)$ and $h_1^d(x)$ do not need to be as large in order to achieve agreement with the A_N^π data. Consequently, if one does *not* include lattice data in the analysis (`JAM3D-22 no LQCD`), the values for $\delta u, \delta d$, and g_T become smaller. The value for δu still agrees with lattice within uncertainties, but δd and g_T are about 1- to 1.5-σ below. However, when the lattice g_T data point is included, as in the full `JAM3D-22` scenario, then one again finds agreement with the lattice results, with $h_1^u(x)$ and $h_1^d(x)$ increasing in magnitude accordingly. This fact conveys an important point: an analysis, at a superficial glance, may appear to have tension with the lattice tensor charge values, but one cannot definitively determine this until lattice data is included. That is, the analysis may be able to find solutions that are compatible with both lattice and experimental data maintaining an acceptable value for the χ^2/npts.

2.4 JAM3D-22* Analysis

We mention that in order to align with the methodology of `JAMDiFF` – see the contribution to these Proceedings from Nobuo Sato ("Transversity from Dihadron Transverse-Spin Observables") – we ran a `JAM3D-22` analysis that is slightly updated from Ref. [1]: antiquark transversity PDFs are now included (with $h_1^{\bar{d}} = -h_1^{\bar{u}}$), a small-$x$ constraint [25] is imposed, and, for the fit with lattice
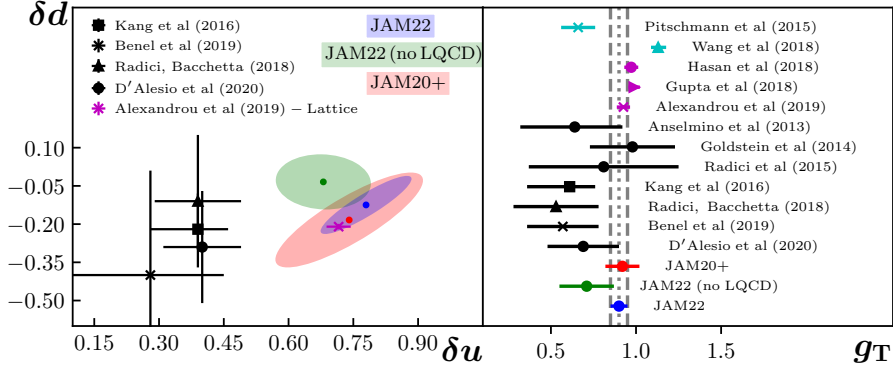
Figure 2: The tensor charges δu, δd, and g_T. Our `JAM3D-22` results (blue) are compared to an analysis that does not include the lattice g_T data point (`JAM3D-22` no LQCD in green) and to the `JAM3D-20+` results (red) along with other results from phenomenology (black), lattice QCD (purple), and Dyson-Schwinger (cyan).

QCD, δu and δd from ETMC [18] and PNDME [26] are used (instead of only the g_T data point from ETMC). The experimental data is still described very well even with including δu and δd from lattice QCD as a Bayesian prior in the fit.

3. Dihadron Fragmentation Theory Developments

3.1 New Definition of DiFFs and Sum Rules

The most common type of FFs describes the situation where a single hadron h is detected in the final state, $i \rightarrow hX$ (X representing all undetected particles). Another intensely studied class of reactions analyzes the case of two hadrons h_1, h_2 being detected from the same parton-initiated jet, $i \rightarrow (h_1 h_2)X$, where dihadron FFs (DiFFs) become relevant. The quantum field-theoretic correlator for the fragmentation of a parton i into two hadrons h_1, h_2, after integrating over k^+, is defined as [27]

$$\Delta_{\alpha\beta}^{h_1 h_2/i}(z_1, z_2, \vec{P}_{1\perp}, \vec{P}_{2\perp}) = \frac{1}{N_i} \sum_X \!\!\!\!\!\!\!\int \frac{d\xi^+ d^2\vec{\xi}_\perp}{(2\pi)^3} e^{ik\cdot\xi} O_{\alpha\beta}^{h_1 h_2/i}(\xi)\Big|_{\xi^-=0}, \tag{8}$$

where z_1, z_2 are the fractions of the parton's longitudinal momentum carried by each hadron, and $\vec{P}_{1\perp}, \vec{P}_{2\perp}$ are the transverse momenta of the hadrons relative to the parton. For a quark, N_i is the number of quark colors $N_c = 3$, and

$$O_{\alpha\beta}^{h_1 h_2/q}(\xi) = \langle 0|\mathcal{W}(\infty,\xi)\psi_{q,\alpha}(\xi^+,0^-,\vec{\xi}_\perp)|P_1,P_2;X\rangle\langle P_1,P_2;X|\bar{\psi}_{q,\beta}(0^+,0^-,\vec{0}_\perp)\mathcal{W}(0,\infty)|0\rangle, \tag{9}$$

where ψ_q is the quark field, α, β are indices for the components of the field, and $\mathcal{W}$ is a Wilson line in the fundamental representation of SU(3) that ensures color gauge invariance. A sum over color indices in Eq. (9) is implied. We will focus on quark fragmentation but analogous results hold for gluons. We will also only consider the production of unpolarized hadron pairs.

For the fragmentation of an unpolarized parton, we parameterize the correlator in Eq. (8) as [28]

$$\frac{1}{64\pi^3 z_1 z_2}\text{Tr}\left[\Delta^{h_1 h_2/q}(z_1, z_2, \vec{P}_{1\perp}, \vec{P}_{2\perp})\gamma^-\right] = D_1^{h_1 h_2/q}(z_1, z_2, \vec{P}_{1\perp}^2, \vec{P}_{2\perp}^2, \vec{P}_{1\perp}\cdot\vec{P}_{2\perp}), \tag{10}$$

where $z = z_1 + z_2$ is the total momentum fraction of the dihadron and $P_h = P_1 + P_2$. To justify that Eq. (10) (and an analogous version for gluon fragmentation) have the desired number density interpretation, we derived sum rules involving our fully unintegrated DiFFs (uDiFFs) in a parton model framework. We focus first on the number sum rule [28],

$$\int d\mathcal{PS}\, D_1^{h_1 h_2/i}(z_1, z_2, \vec{P}_{1\perp}^2, \vec{P}_{2\perp}^2, \vec{P}_{1\perp}\cdot\vec{P}_{2\perp}) = \langle \mathcal{N}(\mathcal{N}-1)\rangle, \tag{11}$$

where $\int d\mathcal{PS} = \sum_{h_1}\sum_{h_2}\int_0^1 dz_2 \int_0^{1-z_2} dz_1 \int d^2\vec{P}_{1\perp}\int d^2\vec{P}_{2\perp}$, and $\mathcal{N}$ is the total number of hadrons produced when the parton i fragments. Thus, $\langle \mathcal{N}(\mathcal{N}-1)\rangle$ is the expectation value for the total number of hadron pairs produced in the fragmentation of i. A sum over hadron spins must be included if either or both hadrons have nonzero spin. We remark that the labeling of the two hadrons as (h_1, h_2) or (h_2, h_1) is distinguishable and no factor of $1/2$ is needed in the r.h.s. of Eq. (11). A crucial step in our proof is being able to introduce the number operator,

$$\hat{N}_{h_j} \equiv \int \frac{dP_j^- d^2\vec{P}_{j\perp}}{(2\pi)^3\, 2P_j^-}\, \hat{a}_{h_j}^\dagger \hat{a}_{h_j} = \int \frac{dz_j d^2\vec{P}_{j\perp}}{(2\pi)^3\, 2z_j}\, \hat{a}_{h_j}^\dagger \hat{a}_{h_j}, \tag{12}$$

for each hadron ($j = 1$ or 2). This can only be achieved by having the specific prefactors on the l.h.s. of Eq. (10). Indeed, a derivation is not possible if a prefactor of $1/(4z) = 1/(4(z_1 + z_2))$ is used on the l.h.s. of Eq. (10).

The result in Eq. (11) gives a clear interpretation for the uDiFF we defined in Eq. (10) [28]: they are densities in the momentum fractions z_1, z_2 and transverse momenta $\vec{P}_{1\perp}, \vec{P}_{2\perp}$ for the number of hadron pairs $(h_1 h_2)$ fragmenting from a parton i. The uDiFF $D_1^{h_1 h_2/q}(z_1, z_2, \vec{P}_{1\perp}^2, \vec{P}_{2\perp}^2, \vec{P}_{1\perp}\cdot\vec{P}_{2\perp})$ encodes the dihadron fragmentation process for an unpolarized quark (γ^- projection of the correlator). The number density interpretation also holds for the fragmentation of a longitudinally polarized quark ($\gamma^-\gamma^5$ projection) and a transversely polarized quark ($i\sigma^{i-}\gamma_5$ projection).

We can also derive a momentum sum rule involving uDiFFs and TMD FFs [28],

$$\sum_{h_1}\int_0^{1-z_2} dz_1 \int d^2\vec{P}_{1\perp}\, z_1\, D_1^{h_1 h_2/i}(z_1, z_2, \vec{P}_{1\perp}^2, \vec{P}_{2\perp}^2, \vec{P}_{1\perp}\cdot\vec{P}_{2\perp}) = (1-z_2)\, D_1^{h_2/i}(z_2, \vec{P}_{2\perp}^2). \tag{13}$$

If either or both hadrons have nonzero spin, then a sum over the spin of h_1 must be included on the l.h.s. of Eq. (13). Note that one can identify the ratio of the uDiFF to the TMD FF, $D_1^{h_1 h_2/i}(z_1, z_2, \vec{P}_{1\perp}^2, \vec{P}_{2\perp}^2, \vec{P}_{1\perp}\cdot\vec{P}_{2\perp})/D_1^{h_2/i}(z_2, \vec{P}_{2\perp}^2)$, as a conditional number density in the momentum $(z_1, \vec{P}_{1\perp})$ for h_1 fragmenting from i given h_2 has fragmented from i with momentum $(z_2, \vec{P}_{2\perp})$.

3.2 Connection to Phenomenology

In order to analyze measurements of dihadron observables, it becomes convenient to change to the "dihadron frame" where the dihadron has no transverse momentum. In addition to $P_h = P_1 + P_2$, we also introduce the relative momentum $R = (P_1 - P_2)/2$. The individual hadrons have masses M_1 and M_2, while the invariant mass (squared) of the dihadron is $M_h^2 = P_h^2$. Along with z, we form the variable $\zeta = (z_1 - z_2)/z$. The hadron momenta P_1 and P_2 can then be written as $P_1 = \left(\frac{M_1^2 + \vec{R}_T^2}{(1+\zeta)P_h^-}, \frac{1+\zeta}{2}P_h^-, \vec{R}_T\right)$ and $P_2 = \left(\frac{M_2^2 + \vec{R}_T^2}{(1-\zeta)P_h^-}, \frac{1-\zeta}{2}P_h^-, -\vec{R}_T\right)$. Note that one readily finds

$\vec{R}_T^2 = \frac{1-\zeta^2}{4}M_h^2 - \frac{1-\zeta}{2}M_1^2 - \frac{1+\zeta}{2}M_2^2$. Due to this change of reference frames, one naturally thinks of uDiFFs as now depending on $(z, \zeta, \vec{k}_T^2, \vec{R}_T^2, \vec{k}_T \cdot \vec{R}_T)$ rather than $(z_1, z_2, \vec{P}_{1\perp}^2, \vec{P}_{2\perp}^2, \vec{P}_{1\perp} \cdot \vec{P}_{2\perp})$.

Nevertheless, the form of the number sum rule in Eq. (11) allows us to generalize the idea of uDiFFs as number densities to any set of variables we choose [28]. Consider making a change of variables from $(z_1, z_2, \vec{P}_{1\perp}, \vec{P}_{2\perp})$ to $(w, x, \vec{Y}, \vec{Z})$, where we understand w, x to be scalars and $\vec{Y}, \vec{Z}$ to be two-dimensional vectors. Then Eq. (11) implies

$$D_1^{h_1 h_2/i}(w, x, \vec{Y}^2, \vec{Z}^2, \vec{Y} \cdot \vec{Z}) \equiv \mathcal{J} \cdot D_1^{h_1 h_2/i}(z_1, z_2, \vec{P}_{1\perp}^2, \vec{P}_{2\perp}^2, \vec{P}_{1\perp} \cdot \vec{P}_{2\perp}) \tag{14}$$

is a number density in $(w, x, \vec{Y}, \vec{Z})$, where $\mathcal{J} = |\partial(z_1, z_2, \vec{P}_{1\perp}, \vec{P}_{2\perp})/\partial(w, x, \vec{Y}, \vec{Z})|$ is the Jacobian for the change of variables from $(z_1, z_2, \vec{P}_{1\perp}, \vec{P}_{2\perp})$ to $(w, x, \vec{Y}, \vec{Z})$. Substituting Eq. (10) into the r.h.s. of Eq. (14) then gives an operator definition of $D_1^{h_1 h_2/i}(w, x, \vec{Y}^2, \vec{Z}^2, \vec{Y} \cdot \vec{Z})$. In addition, integrating over one or more of the variables $(w, x, \vec{Y}, \vec{Z})$ will define a DiFF that is a number density in the remaining variables.

The functions of interest in experimental measurements are the so-called "extended DiFFs" (extDiFFs), which we define by changing variables from $(z_1, z_2, \vec{P}_{1\perp}, \vec{P}_{2\perp})$ to $(z, \zeta, \vec{k}_T, \vec{R}_T)$ (as above) and integrating over $\vec{k}_T$. In the quark sector, two twist-2 Dirac projections survive [27, 29]:

$$\frac{z}{32\pi^3(1-\zeta^2)}\int d^2\vec{k}_T \, \mathrm{Tr}\Big[\Delta^{h_1 h_2/q}(z_1, z_2, \vec{P}_{1\perp}, \vec{P}_{2\perp})\gamma^-\Big] = D_1^{h_1 h_2/q}(z, \zeta, \vec{R}_T^2), \tag{15}$$

$$\frac{z}{32\pi^3(1-\zeta^2)}\int d^2\vec{k}_T \, \mathrm{Tr}\Big[\Delta^{h_1 h_2/q}(z_1, z_2, \vec{P}_{1\perp}, \vec{P}_{2\perp})i\sigma^{i-}\gamma_5\Big] = -\frac{\epsilon_T^{ij}R_T^j}{M_h}H_1^{\sphericalangle\, h_1 h_2/q}(z, \zeta, \vec{R}_T^2), \tag{16}$$

where $\epsilon_T^{ij} = \epsilon^{-+ij}$ with $\epsilon_T^{12} = 1$. We emphasize the existence of $H_1^{\sphericalangle\, h_1 h_2/q}(z, \zeta, \vec{R}_T^2)$, which is not present for fragmentation into a single hadron. This function has become important in the extraction of the transversity PDFs, which couple to it in dihadron observables [20, 22, 23, 30–35].

Experimental measurements of dihadron observables are usually differential in (z, M_h) and integrated over ζ. The relevant DiFFs are then dependent on (z, M_h). We change variables from $(z_1, z_2, \vec{P}_{1\perp}, \vec{P}_{2\perp})$ to $(z, \zeta, \vec{k}_T, M_h, \phi_{R_T})$, where ϕ_{R_T} is the azimuthal angle of $\vec{R}_T$. The Jacobian is $\mathcal{J} = z^3(1-\zeta^2)/8$. Using our aforementioned prescription, we can define a DiFF that is a number density in (z, M_h):

$$D_1^{h_1 h_2/i}(z, M_h) \equiv \frac{\pi}{2}M_h \int_{-1}^1 d\zeta \, (1-\zeta^2)D_1^{h_1 h_2/i}(z, \zeta, \vec{R}_T^2). \tag{17}$$

3.3 Parton Model Cross Section Results for $e^+e^- \to (h_1\, h_2)\, X$

Actually, calculating the leading-order cross section for $d\sigma/dz\, dM_h$ for $e^+e^- \to (h_1 h_2)X$ serves as another verification of the number density interpretation of our new definition of $D_1^{h_1 h_2/i}(z, M_h)$. Starting from $P_1^0 P_2^0 \, d\sigma/d^3\vec{P}_1 d^3\vec{P}_2$, the result takes the form [28]

$$\frac{d\sigma}{dz\, dM_h} = \hat{\sigma}_0^i \, D_1^{h_1 h_2/i}(z, M_h). \tag{18}$$

For $i = q$, $\hat{\sigma}_0^q = 4\pi\alpha_{\mathrm{em}}^2 N_c e_q^2/(3s)$, which is the partonic cross section for $e^+e^- \to \gamma \to q\bar{q}$, where α_{em} is the fine structure constant, and $\sqrt{s}$ is the center-of-mass energy of the e^+e^- pair.

A sum over quarks and antiquarks is then needed on the r.h.s. of Eq. (18). For $i = g$, $\hat{\sigma}_0^g = [(\alpha_s^2 G_F^2)/(576\pi^3)][(m_e^2 s^2 (N_c^2 - 1))/(s - m_H^2)^2]$, which is the partonic cross section for $e^+ e^- \to H \to gg$ (H being the Higgs boson) using an effective H-g-g coupling, α_s is the strong coupling, G_F is the Fermi constant, and m_e (m_H) is the mass of the electron (Higgs). A factor of 2 is now needed on the r.h.s. of Eq. (18) since both gluons have the ability to fragment into the dihadron. The structure of Eq. (18) is exactly what one expects if $D_1^{h_1 h_2/i}(z, M_h)$ is to be interpreted as a number density, i.e., the differential cross section equals the total partonic cross section times the DiFF. We have also explicitly confirmed this feature for other sets of variables, including $d\sigma/dz_1 dz_2$ and $d\sigma/dz\, d\zeta\, d^2\vec{R}_T$ involving $D_1^{h_1 h_2/i}(z_1, z_2)$ and $D_1^{h_1 h_2/i}(z, \zeta, \vec{R}_T^2)$, respectively.

3.4 Evolution Equations for DiFFs

The evolution of the DiFF correlator in Eq. (8) has two pieces: a "homogeneous term" involving only DiFFs (an example graph is given in Fig. 3(a)), and an "inhomogeneous term" involving single-hadron FFs (an example graph is given in Fig. 3(b)). We have explicitly checked that the inhomogeneous term for the evolution of $D_1^{h_1 h_2/i}(z, \zeta, \vec{R}_T^2)$ is not ultraviolet divergent, and therefore does not contribute to the evolution of extDiFFs. The same conclusion was reached in Ref. [36]. We also remark that for extDiFFs, inhomogeneous diagrams will contribute at $O(\alpha_s^2)$ and higher orders of evolution.

For collinear PDFs and FFs (e.g., $f_1^{i/N}(x)$ and $D_1^{h/i}(z)$), evolution is a perturbative process for the $1 \to 2$ splitting of a parton and is independent of the target (in the case of PDFs) or final state (in the case of FFs) – see, e.g., Ref. [37] Secs. 9.3.1, 12.9. This observation, along with the structure of the correlator in Eq. (8), the fact that the extDiFFs are obtained by integrating over $\vec{k}_T$, and the conclusion that only the homogeneous term contributes to their evolution, makes clear that the splitting functions for extDiFFs will be the same as those for a parton fragmenting into a single hadron. The final result reads [28]

$$\frac{\partial \mathcal{D}^{h_1 h_2/i}(z, \zeta, \vec{R}_T^2; \mu)}{\partial \ln \mu^2} = \sum_{i'} \int_z^1 \frac{dw}{w} \mathcal{D}^{h_1 h_2/i'}\left(\frac{z}{w}, \zeta, \vec{R}_T^2; \mu\right) P_{i \to i'}(w), \tag{19}$$

where $\mathcal{D} = D_1$ or $H_1^{\sphericalangle}$, and $P_{i \to i'}(w)$ are the unpolarized time-like splitting kernels when $\mathcal{D} = D_1$, or the transversely polarized splitting kernels when $\mathcal{D} = H_1^{\sphericalangle}$. We note that $D_1^{h_1 h_2/i}(z, M_h)$ and $H_1^{\sphericalangle\, h_1 h_2/i}(z, M_h)$ obey the same evolution equations as Eq. (19) since the ζ dependence there is not altered in the evolution.

4. Summary

We have performed a global analysis of TSSAs (JAM3D-22) using the Sivers $A_{UT}^{\sin(\phi_h - \phi_S)}$, Collins $A_{UT}^{\sin(\phi_h + \phi_S)}$, and $A_{UT}^{\sin\phi_S}$ asymmetries in SIDIS, Collins asymmetry in SIA for so-called unlike-like (A_{UL}) and unlike-charged (A_{UC}) ratios, Sivers asymmetry in DY for $W^\pm/Z$ production ($A_N^{W/Z}$) and for $\mu^+\mu^-$ production ($A_{T,\mu^+\mu^-}^{\sin\phi_S}$), and A_N for pion production in proton-proton collisions (A_N^π). as well as constraints from lattice QCD (tensor charge g_T) and the Soffer bound on transversity. Our JAM3D-22 results show it is still possible to accommodate these data/constraints and describe all TSSAs. The newly extracted transversity function and associated tensor charges are much
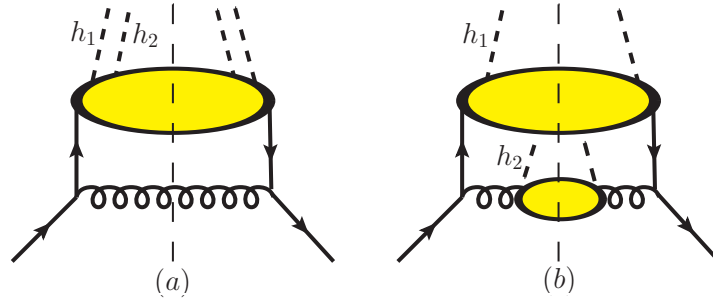
Figure 3: Example diagrams of the (a) homogeneous and (b) inhomogeneous terms for the evolution of the extDiFF $D_1^{h_1 h_2/q}(z, \zeta, \vec{R}_T^2)$.

more precise. We also have the first direct information from experiment on $\tilde{H}(z)$. We have introduced a new definition of dihadron fragmentation functions that is consistent with a number density interpretation, giving these functions a clear physical meaning, and derived their associated evolution equations.

References

[1] L. Gamberg *et al.* [Jefferson Lab Angular Momentum (JAM) and Jefferson Lab Angular Momentum], Phys. Rev. D **106**, no.3, 034014 (2022) [arXiv:2205.00999 [hep-ph]].

[2] P. Herczeg, Prog. Part. Nucl. Phys. **46**, 413-457 (2001)

[3] J. Erler and M. J. Ramsey-Musolf, Prog. Part. Nucl. Phys. **54**, 351-442 (2005) [arXiv:hep-ph/0404291 [hep-ph]].

[4] N. Severijns, M. Beck and O. Naviliat-Cuncic, Rev. Mod. Phys. **78**, 991-1040 (2006) [arXiv:nucl-ex/0605029 [nucl-ex]].

[5] V. Cirigliano, S. Gardner and B. Holstein, Prog. Part. Nucl. Phys. **71**, 93-118 (2013) [arXiv:1303.6953 [hep-ph]].

[6] A. Courtoy, S. Baeßler, M. González-Alonso and S. Liuti, Phys. Rev. Lett. **115**, 162001 (2015) [arXiv:1503.06814 [hep-ph]].

[7] M. González-Alonso, O. Naviliat-Cuncic and N. Severijns, Prog. Part. Nucl. Phys. **104**, 165-223 (2019) [arXiv:1803.08732 [hep-ph]].

[8] M. Pospelov and A. Ritz, Annals Phys. **318**, 119-169 (2005) [arXiv:hep-ph/0504231 [hep-ph]].

[9] N. Yamanaka, B. K. Sahoo, N. Yoshinaga, T. Sato, K. Asahi and B. P. Das, Eur. Phys. J. A **53**, no.3, 54 (2017) [arXiv:1703.01570 [hep-ph]].

[10] T. Liu, Z. Zhao and H. Gao, Phys. Rev. D **97**, no.7, 074018 (2018) [arXiv:1704.00113 [hep-ph]].

[11] A. Accardi, L. T. Brady, W. Melnitchouk, J. F. Owens and N. Sato, Phys. Rev. D **93**, no.11, 114017 (2016) [arXiv:1602.03154 [hep-ph]].

[12] D. de Florian, R. Sassot and M. Stratmann, Phys. Rev. D **76**, 074033 (2007) [arXiv:0707.1506 [hep-ph]].

[13] P. C. Barry, N. Sato, W. Melnitchouk and C. R. Ji, Phys. Rev. Lett. **121**, no.15, 152001 (2018) [arXiv:1804.01965 [hep-ph]].

[14] D. W. Duke and J. F. Owens, Phys. Rev. D **30**, 49-54 (1984)

[15] C. Cocuzza *et al.* [Jefferson Lab Angular Momentum (JAM)], Phys. Rev. D **106**, no.3, L031502 (2022) [arXiv:2202.03372 [hep-ph]].

[16] L. Gamberg *et al.* [Jefferson Lab Angular Momentum (JAM)], https://colab.research.google.com/github/pitonyak25/jam3d_dev_lib/blob/main/JAM3D_Library.ipynb

[17] L. Gamberg *et al.* [Jefferson Lab Angular Momentum (JAM)], https://github.com/pitonyak25/jam3d_dev_lib/tree/main/LHAPDF_tables

[18] C. Alexandrou, S. Bacchio, M. Constantinou, J. Finkenrath, K. Hadjiyiannakou, K. Jansen, G. Koutsou and A. Vaquero Aviles-Casco, Phys. Rev. D **102**, no.5, 054517 (2020) [arXiv:1909.00485 [hep-lat]].

[19] M. Anselmino, M. Boglione, U. D'Alesio, S. Melis, F. Murgia and A. Prokudin, Phys. Rev. D **87**, 094019 (2013) [arXiv:1303.3822 [hep-ph]].

[20] M. Radici, A. Courtoy, A. Bacchetta and M. Guagnelli, JHEP **05**, 123 (2015) [arXiv:1503.03495 [hep-ph]].

[21] Z. B. Kang, A. Prokudin, P. Sun and F. Yuan, Phys. Rev. D **93**, no.1, 014009 (2016) [arXiv:1505.05589 [hep-ph]].

[22] M. Radici and A. Bacchetta, Phys. Rev. Lett. **120**, no.19, 192001 (2018) [arXiv:1802.05212 [hep-ph]].

[23] J. Benel, A. Courtoy and R. Ferro-Hernandez, Eur. Phys. J. C **80**, no.5, 465 (2020) [arXiv:1912.03289 [hep-ph]].

[24] U. D'Alesio, C. Flore and A. Prokudin, Phys. Lett. B **803**, 135347 (2020) [arXiv:2001.01573 [hep-ph]].

[25] Y. V. Kovchegov and M. D. Sievert, Phys. Rev. D **99**, no.5, 054033 (2019) [arXiv:1808.10354 [hep-ph]].

[26] R. Gupta, B. Yoon, T. Bhattacharya, V. Cirigliano, Y. C. Jang and H. W. Lin, Phys. Rev. D **98**, no.9, 091501 (2018) [arXiv:1808.07597 [hep-lat]].

[27] A. Bianconi, S. Boffi, R. Jakob and M. Radici, Phys. Rev. D **62**, 034008 (2000) [arXiv:hep-ph/9907475 [hep-ph]].

[28] D. Pitonyak, C. Cocuzza, A. Metz, A. Prokudin and N. Sato, Phys. Rev. Lett. **132**, no.1, 011902 (2024) [arXiv:2305.11995 [hep-ph]].

[29] J. C. Collins, S. F. Heppelmann and G. A. Ladinsky, Nucl. Phys. B **420**, 565-582 (1994) [arXiv:hep-ph/9305309 [hep-ph]].

[30] A. Bacchetta, A. Courtoy and M. Radici, Phys. Rev. Lett. **107**, 012001 (2011) [arXiv:1104.3855 [hep-ph]].

[31] A. Courtoy, A. Bacchetta, M. Radici and A. Bianconi, Phys. Rev. D **85**, 114023 (2012) [arXiv:1202.0323 [hep-ph]].

[32] A. Bacchetta, A. Courtoy and M. Radici, JHEP **03**, 119 (2013) [arXiv:1212.3568 [hep-ph]].

[33] M. Radici, A. M. Ricci, A. Bacchetta and A. Mukherjee, Phys. Rev. D **94**, no.3, 034012 (2016) [arXiv:1604.06585 [hep-ph]].

[34] C. Cocuzza *et al.* [JAM], Phys. Rev. Lett. **132**, no.9, 091901 (2024) [arXiv:2306.12998 [hep-ph]].

[35] C. Cocuzza *et al.* [Jefferson Lab Angular Momentum (JAM)], Phys. Rev. D **109**, no.3, 034024 (2024) [arXiv:2308.14857 [hep-ph]].

[36] F. A. Ceccopieri, M. Radici and A. Bacchetta, Phys. Lett. B **650**, 81-89 (2007) [arXiv:hep-ph/0703265 [hep-ph]].

[37] J. Collins, Camb. Monogr. Part. Phys. Nucl. Phys. Cosmol. **32**, 1-624 (2011) Cambridge University Press, 2023, ISBN 978-1-009-40184-5, 978-1-009-40183-8, 978-1-009-40182-1 doi:10.1017/9781009401845